

# Semi-synthetic zigzag optical lattice for ultracold bosons

E. Anisimovas,<sup>1,\*</sup> M. Račiūnas,<sup>1</sup> C. Sträter,<sup>2,†</sup> A. Eckardt,<sup>2,‡</sup> I. B. Spielman,<sup>3,4,§</sup> and G. Juzeliūnas<sup>1,¶</sup>

<sup>1</sup>*Institute of Theoretical Physics and Astronomy,  
Vilnius University, Saulėtekio 3, LT-10222 Vilnius, Lithuania*

<sup>2</sup>*Max-Planck-Institut für Physik komplexer Systeme,  
Nöthnitzer Straße 38, D-01187 Dresden, Germany*

<sup>3</sup>*Joint Quantum Institute, University of Maryland, College Park, Maryland 20742-4111, USA*

<sup>4</sup>*National Institute of Standards and Technology, Gaithersburg, Maryland 20899, USA*

(Dated: June 4, 2022)

We consider a one-dimensional “zigzag” lattice, pictured as a two-site wide single strip taken from a triangular lattice, affected by a tunable homogeneous magnetic flux piercing its triangular plaquettes. We focus on a semi-synthetic lattice produced by combining a one-dimensional spin-dependent lattice in the long direction with laser-induced transitions between atomic internal states that define the short synthetic dimension. In contrast to previous studies on semi-synthetic lattices, the atom-atom interactions are nonlocal in both lattice directions. We investigate the ground-state properties of the system for the case of strongly interacting bosons, and find that the interplay between the frustration induced by the magnetic field and the interactions gives rise to an exotic gapped phase at fractional filling factors corresponding to one particle per magnetic unit cell.

PACS numbers: 73.43.-f, 67.85.-d, 71.10.Hf

Optical lattices provide a unique tool for simulating quantum condensed matter physics using ultracold atoms [1–3]. These lattices can be enriched by introducing laser-coupled internal atomic states [4–9] that can play the role of an extra “synthetic” dimension [10–12]. For example, a semi-synthetic square lattice results from the combination of the interlayer tunneling among the sites of a one-dimensional optical lattice and laser-assisted transitions between the onsite atomic levels. If the laser coupling is accompanied by a recoil in the lattice direction, the semi-synthetic lattice acquires a uniform magnetic flux traversing the square plaquettes [11]. This leads to the formation of chiral edge states in the resulting quantum Hall ribbon [11, 13–16]. A characteristic feature of the square geometry is that the atom-atom interaction is long-ranged in the synthetic dimension but short-ranged in the real dimension [11, 17–19].

In this Letter, we find the ground states of a semi-synthetic optical zigzag lattice which can be created combining a spin-dependent one-dimensional optical lattice with laser-induced transitions between the atomic internal states [20]. The lattice is affected by a tunable homogeneous magnetic flux and features nonlocal interactions both in the synthetic and the real dimensions. Nonlocal interactions are an important goal in recent experiments, and previously such interactions have been engineered via superexchange [21–24] dipole-dipole coupling [25–28], or Rydberg dressing [29–32]. We numerically investigate the ground-state properties of the proposed system for the case of bosonic atoms with strong interactions using the density-matrix renormalization group [33–35] calculations. We find that the interplay between the frustration induced by the magnetic field and the interactions gives rise to an exotic gapped phase at fractional per-site filling fractions, where there is one particle per magnetic

unit cell.

*Single-particle Hamiltonian.*—We consider bosonic atoms with two relevant internal states labeled with the (quasi-)spin index  $s = \pm 1$ . The atoms are confined in one-dimensional periodic trapping potentials, opposite for each internal state,  $V \propto \pm \cos(\kappa x)$ . In addition, the two quasi-spin states are coupled by laser-induced transitions characterized by a Rabi frequency  $\Omega$  and a recoil wave vector  $\tilde{\kappa} \mathbf{e}_x$  aligned along the lattice direction  $\mathbf{e}_x$ . The resulting single-particle Hamiltonian is

$$H = \frac{\hat{p}^2}{2m} + \frac{V_0}{2} \cos(\kappa x) \sigma_z + \hbar \Omega (\sigma_+ e^{i\tilde{\kappa}x} + \sigma_- e^{-i\tilde{\kappa}x}), \quad (1)$$

where  $V_0$  is the height of the trapping potential, and  $\sigma_z$  and  $\sigma_{\pm} = \sigma_x \pm i\sigma_y$  denote the standard Pauli spin matrices and combinations thereof.

The out-of-phase optical lattice can be produced using the ground state  $^1S_0$  and the long-lived excited state  $^3P_0$  of the alkaline-earth(-like) atoms, such as Ytterbium [15] or Strontium [39, 40], for which the excited state has a typical lifetime far exceeding the experimental time scale [7, 15, 39, 41]. In contrast to the recent experiments [15, 39], the atoms are to be trapped at an anti-magic (rather than magic) wavelength to have the opposite trapping potentials for the two atomic internal states. Alternatively, one may also use two Raman-coupled hyperfine atomic states  $|F, m_F\rangle$  with projections  $m_F = 0$  and  $m_F = -1$  from the  $F = 1$  ground-state manifold of the  $^{87}\text{Rb}$  atoms [42]. The lattice potential  $V \propto \pm \cos(\kappa x)$  is then obtained by balancing the vector and scalar light shifts of a state-dependent lattice [8, 37]. This can be done by using a standing wave of a circularly (either  $\sigma_+$  or  $\sigma_-$ ) polarized light, and detuning slightly away from the frequency at which the scalar light shift is exactly zero.

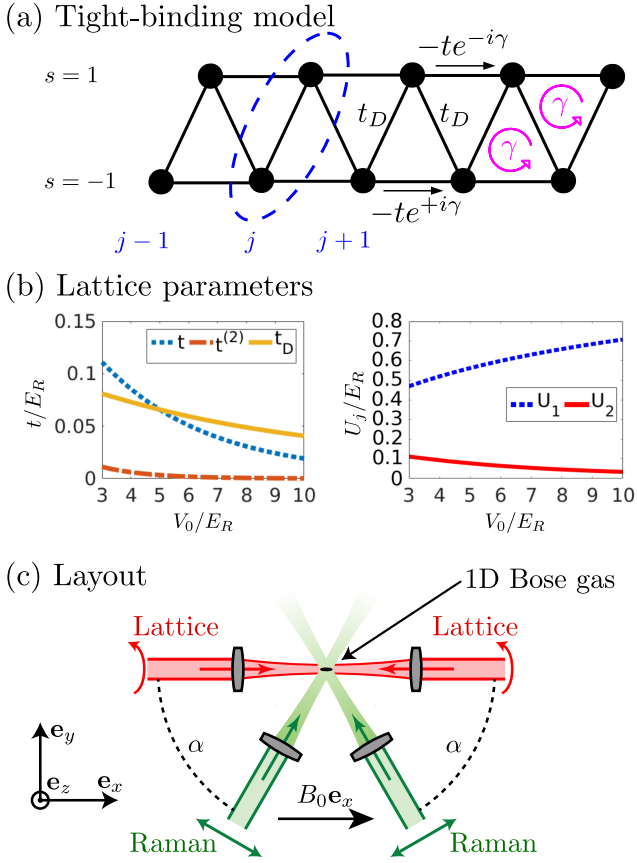


FIG. 1. (a) The semi-synthetic zigzag lattice corresponding to the tight-binding Hamiltonian (2). (b) Tight-binding parameters. Left: Horizontal nearest neighbor ( $t$ ) and next-nearest neighbor ( $t^{(2)}$ ) hopping parameters together with diagonal tunneling strength  $t_D$  as a function of the lattice depth  $V_0/E_R$  for  $\Omega = 0.2020 E_R$ ; Right: Normalized interactions  $U_1$  and  $U_2$  [36] as a function of the lattice depth. (c) Schematic layout of a possible experimental setup. A bias magnetic field  $B_0 e_x$  Zeeman-splits the hyperfine spin states of  $^{87}\text{Rb}$  atoms. A counterpropagating pair of  $\sigma_+$ -polarized laser beams with  $\lambda_L \approx 789$  nm form a spin-dependent lattice [8, 37, 38]. It traps the  $|F=1, m_F=-1, 0\rangle$  states on lattice sites shifted by half the lattice constant providing a semi-synthetic zigzag lattice. Two horizontally polarized lasers at  $\lambda_R \approx 790$  nm resonantly couple the two spin states producing the flux  $\gamma = \pi/2$  for the angle between the laser beams  $\alpha \approx 60^\circ$ .

Here we focus on sufficiently deep lattices, with the lattice depth  $V_0$  typically exceeding the recoil energy  $E_R = \hbar^2 \kappa^2 / 8m$  five times. In this regime, a tight-binding approach is appropriate, and the internal states  $s = \pm 1$  are interpreted as sites along the synthetic dimension [11]. The bosonic operators  $c_{s,j}^\dagger$  ( $c_{s,j}$ ) create (annihilate) atoms on the sites of the resulting semi-synthetic zigzag lattice depicted in Fig. 1(a), where  $j$  labels the sites along the physical (long) direction. Due to the recoil the triangular plaquettes of the lattice are pierced by a uniform flux  $\gamma = \pi \tilde{\kappa} / \kappa = a \tilde{\kappa} / 2$ , with  $a = 2\pi / \kappa$  being the lattice constant. Absorbing the appropriate phases into the

onsite Wannier functions, the tight-binding Hamiltonian can be described in terms of complex-valued tunneling parameters  $-t e^{\pm i\gamma}$  along the long direction and real-valued parameters  $t_D$  along the diagonal semi-synthetic directions [36]

$$H = t_D \sum_{\langle jj' \rangle} c_{1,j}^\dagger c_{-1,j'} - t \sum_{j,m} c_{m,j+1}^\dagger c_{m,j} e^{-ima\tilde{\kappa}/2} + \text{h.c.} \quad (2)$$

Here, the shorthand  $\langle jj' \rangle$  indicates the summation over all values of  $j$  while restricting the values of  $j'$  to either  $j$  or  $j+1$ , thus enumerating all diagonal (in the semi-synthetic space) spin-raising transitions. The tunneling amplitude  $t_D = \Omega \rho > 0$  is determined by both the laser Rabi frequency  $\Omega$  and the overlap integral  $\rho$  between the neighboring Wannier functions [36].

Figure 1(b) displays the dependence of the tunneling parameters  $t$  and  $t_D$  on the lattice depth for the characteristic value of the Rabi frequency  $\Omega = 0.2020 E_R$ . This particular choice of the laser strength leads to equal values of the two hopping parameters  $t = t_D$  for the lattice depth  $V_0 = 5 E_R$  used in our calculations. Note that the ratio  $t_D/t$  is tunable and increases linearly with the Rabi frequency  $\Omega$ . Couplings between more distant sites are much smaller and can safely be neglected.

In terms of the momentum-space bosonic operators  $\hat{c}_{s,k}^{(\dagger)}$  the Hamiltonian reads

$$H = \sum_k \begin{pmatrix} \hat{c}_{1,k}^\dagger & \hat{c}_{-1,k}^\dagger \end{pmatrix} \begin{pmatrix} h_{11} & h_{12} \\ h_{21} & h_{22} \end{pmatrix} \begin{pmatrix} \hat{c}_{1,k} \\ \hat{c}_{-1,k} \end{pmatrix}, \quad (3)$$

where  $h_{12} = h_{21} = 2t_D \cos(ka/2)$  and  $h_{jj} = -2t \cos[ka + \gamma(-1)^j]$ , with the row index  $j = 1, 2$ . To develop some intuition into the single-particle properties of the model, let us look at the case where  $\tilde{\kappa} = \kappa/2$ . The flux over a triangular plaquette is then  $\gamma = \pi/2$ , so that the time-reversal symmetry is broken even though the flux over a single elementary cell evaluates to  $2\gamma = \pi$ . (On the other hand, the time-reversal symmetry is preserved if the triangular plaquette of the zigzag lattice is pierced by a  $\pi$  flux [43].) For the specific value of  $\gamma = \pi/2$  the two dispersion branches read

$$\epsilon_{\pm}(k) = \pm 2 \sqrt{t^2 \sin^2(ka) + t_D^2 \cos^2(ka/2)}. \quad (4)$$

The tight-binding dispersion (4) is in a good agreement with the exact band structure shown in Fig. 2 for the zigzag lattice with  $\tilde{\kappa} = \kappa/2$  and  $V_0 = 5 E_R$  corresponding to  $t = 0.0658 E_R$  and  $\rho = 0.3258$ , with different values of  $\Omega$  determining  $t_D = \Omega \rho$ . It is noteworthy that the dispersion becomes quartic around  $k = 0$  for  $t_D = t_{D,\text{critical}} = 2t$  corresponding to the critical Rabi frequency  $\Omega_{\text{critical}} = 2t/\rho$ . For the lattice depth  $V_0 = 5 E_R$  the critical Rabi frequency is  $\Omega_{\text{critical}} = 0.4039 E_R$ , and the resulting band structure is shown in Fig. 2(c). Below the critical value,  $t_D < 2t$ , there are two symmetric minima at  $k = \pm \arccos[(t_D/2t)^2]$ . Above the

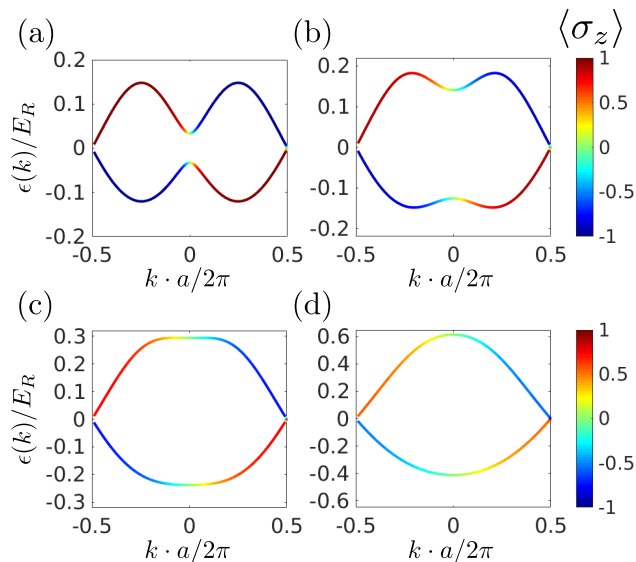


FIG. 2. Exactly calculated dispersion curves for  $V_0 = 5 E_R$ ,  $\kappa = 2\tilde{\kappa}$  ( $\gamma = \pi/2$ ) and various strengths of the spin-flip coupling: (a)  $\Omega = 0.05$ , (b)  $\Omega = 0.2020$ , (c)  $\Omega = 0.4039 E_R$  (the critical value), and (d)  $\Omega = 0.8 E_R$ . This corresponds to: (a)  $t_D = 0.25t$ , (b)  $t_D = t$ , (c)  $t_D = 2t$  (quartic dispersion at  $k = 0$ ), and (d)  $t_D = 4t$ .

critical value,  $t_D > 2t$ , there is a single minimum at  $k = 0$ . We stress that the plots represent the exact calculations which agree well the tight-binding model for  $\Omega$  up to the critical value  $\Omega_{\text{critical}}$  and a little above it. Yet for  $\Omega = 0.8 E_R \approx 2\Omega_{\text{critical}}$  (i.e. for  $\Omega\rho \approx 4t$ ), there is already a quite clear deviation from the tight-binding model. This is approximately the regime where Zhou and Cui [44] also saw deviations from the tight-binding model for a square semi-synthetic lattice.

The spin magnetization  $\langle \sigma_z \rangle$  of the eigenstates is indicated by color in Fig. 2. The red and blue colors correspond to a fully magnetized state with  $s = 1$  and  $s = -1$ , respectively. In the case of weak coupling (upper panels) the dispersion has a double-well shape with a clear spin separation in different minima. For stronger coupling the spin states get increasingly mixed. At the critical value  $\Omega = 0.4039 E_R$ , the double well transforms to a single-minimum shape with a strong spin mixture.

A characteristic feature of the zigzag lattice is the crossing of the two energy bands at the edges of the Brillouin zone (BZ)  $ka = \pm\pi$ . In Fig. 2 we see that there is no band gap at these points and the spin polarization is preserved when moving from one energy band to the other at the BZ boundary. This is also true for other values of  $\gamma$ . It is a consequence of the invariance of the Hamiltonian (1) under the spatial translation by half the lattice period  $a/2$  followed by time reversal, the latter representing a spin flip combined with an inversion of the Peierls phase  $\gamma \rightarrow -\gamma$ . As a result, the period of Bloch oscillations is doubled [36, 45].

*Many-body simulations.*—In addition to the characteristic bosonic onsite interactions, the semi-synthetic zigzag lattice also supports nearest-neighbor repulsion between opposite spin states. The relative magnitudes of the respective interaction energies,  $U_1$  and  $U_2$  are shown in Fig. 1 (b) for a range of lattice heights. In our calculations we specialize to the lattice height  $V_0 = 5 E_R$  where  $U_1 \approx 0.56 E_R$  and  $U_2 \approx 0.074 E_R$ .

To investigate the many-body phases supported by the semi-synthetic zigzag lattice we performed a series of numerical simulations based on the density-matrix renormalization group technique [34] using the open-source OSMPS code [46]. Our simulations targeted the ground states of lattices containing  $L = 60$  sites (that is, 30 two-site unit cells) with open boundary conditions and fractional filling factors  $N/L$  corresponding to all integer particle numbers  $N$  up to 60. Working with such finite systems we were able to stay close to the experimentally feasible regime [47] while also maintaining a reasonable numerical effort. To check the scaling properties of the obtained results representative simulations were rerun also with larger lattice sizes containing up to 120 sites. The remaining two parameters whose values were tuned in a broad interval are the flux  $\gamma$  and the diagonal hopping parameter  $t_D$ . On the other hand, the values for the horizontal hopping parameter  $t \approx 0.066 E_R$  and the nearest-neighbor interaction strength  $U_2$  were taken from the modeling of a lattice of depth  $V_0 = 5 E_R$  [cf. Fig. 1(b)]. Focusing on the effects brought about by the strong atom-atom interactions, in the main part of our calculations we chose to work in the limit of hardcore bosons. Thus, the onsite interaction strength  $U_1 \approx 0.56 E_R$  is regarded to be the dominant energy scale and is accounted for by restricting the number of bosons per lattice site to be not more than one. Having rerun the calculations with more than one boson per site we were able to confirm that the observed interesting many-body phases described below are indeed adequately represented by the hardcore limit.

The zigzag lattice offers a possibility to realize a tunable single-particle dispersion, seen in Fig. 2, by changing the ratio of the diagonal and horizontal tunneling parameters  $t_D/t$ . In the limits where one of the hopping strengths significantly exceeds the other, we observe quasicondensed phases signaled by the algebraic decay of the single-particle density matrix  $g_1(i, j) \equiv \langle c_i^\dagger c_j \rangle$  as a function of the separation of sites  $|i - j|$  [48]. In the limit of a dominant diagonal tunneling  $t_D$ , one obtains the usual quasicondensate at the single minimum at  $k = 0$ . Since the magnetic flux is not absorbed into the internal structure of the quasicondensate wave function with  $k = 0$ , the chiral currents are induced in the legs of the lattice [47, 49]. This phase supported by the zigzag lattice corresponds to the one observed in square ladders [47, 49]. It has been termed the *Meissner phase* in analogy to the physics of superconductors. In the opposite

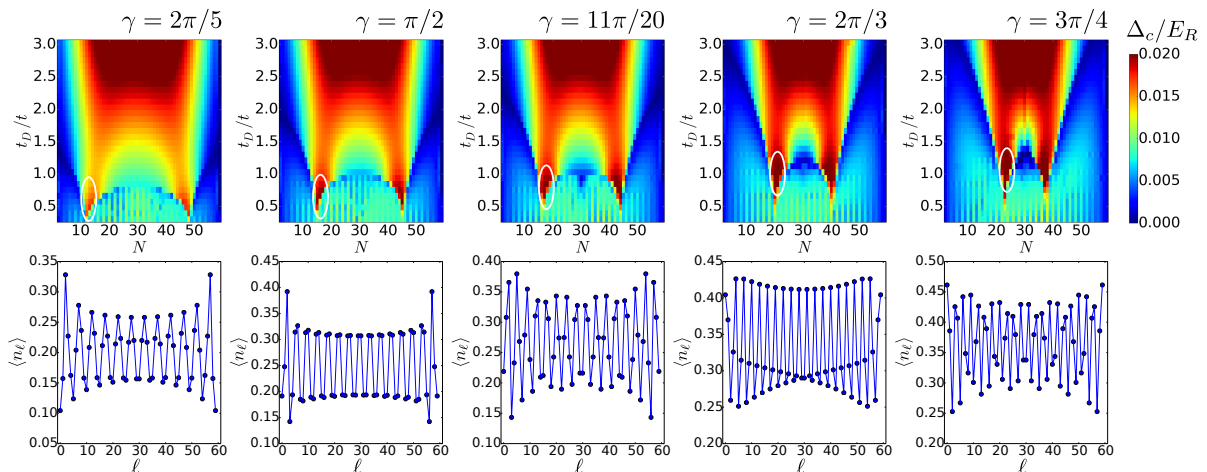


FIG. 3. Many-body phase diagram of the zigzag lattice for a set of flux values  $\gamma = \{0.4\pi, 0.5\pi, 0.55\pi, \frac{2}{3}\pi, \frac{3}{4}\pi\}$ . Top row: the scaled charge gap  $\Delta_c/E_R$  plotted as a function of the number of particles  $N$  in the lattice of size  $L = 60$  and the ratio of the hopping strengths  $t_D/t$ . Areas corresponding to enhanced charge gaps close to  $t_D \approx t$  and the filling factor  $N/L = \gamma/2\pi$  are conspicuous and are marked with white ovals. Bottom row: the expectation of the site occupation  $\langle n_\ell \rangle$  versus the site number  $\ell$  calculated at the phase-diagram points inside the white ovals.

limit of weakly coupled spin-polarized legs – that is, when the horizontal hopping  $t$  is dominant – we find a striped phase analogous to the *vortex phase* formed in square ladders [47, 49]. Here, the current and density oscillations are induced by the interference of partial quasicondensates occupying the two minima in the single-particle band structure. While this qualitative picture is strictly valid for non-interacting bosons it does survive also in the presence of finite interactions. Let us also stress that in the thermodynamic limit (as opposed to finite-size simulations) the gapless vortex phase is expected to support oscillations in the density correlations and not the density itself.

In between the two limits supporting quasicondensed ground states there lies an intriguing regime of balanced tunneling strengths  $t \sim t_D$  associated with the presence of kinetic frustration. In particular, when  $t = t_D$  each triangular plaquette is characterized by the absence of a weak link that could absorb the complex phase accumulated while encircling the plaquette. Under such circumstances the role of the atom-atom interactions will be enhanced, which might drive the system into a gapped phase. Indeed, our simulations show that the power-law decay of the single-particle density matrix  $g_1(i, j)$  is replaced by an exponential decay signaling the destruction of the quasicondensed phase. To complement these observations, in Fig. 3 we plot the behavior of the charge gap [50]  $\Delta_c(N) = E_{N+1} + E_{N-1} - 2E_N$  calculated from the ground-state energies of the zigzag lattice with a varying number of particles. In the top row, the coordinate axes represent the two governing parameters, the filling factor  $N/L$  (with  $L = 60$ ) plotted on the horizontal axis and the ratio of the hopping parameters  $t_D/t$  plotted on the vertical axis. The series of five phase diagrams

represent a subset of calculations performed on a dense set of different values of the flux  $\gamma$ .

The phase diagrams reveal the emergence of areas – marked with white ovals – where charge gaps are significantly enhanced. It is noteworthy that these gapped “islands” are situated precisely at the parameter values where the single-particle correlations decay exponentially and the filling factor assumes flux-dependent values  $N/L = \gamma/2\pi$  and  $N/L = 1 - \gamma/2\pi$ . These two values are related by the particle-hole symmetry brought about by the hardcore constraint. They correspond precisely to the situation with one particle or hole per magnetic unit cell containing  $2\pi/\gamma$  triangular lattice plaquettes or  $2\pi/\gamma$  sites, like in the integer bosonic Hall effect [51–54]. The bottom row of panels in Fig. 3 shows the particle density oscillations calculated at points taken from inside the white ovals. Here, the expectation value of the density  $\langle n_\ell \rangle$  is plotted as a function of the site index  $0 \leq \ell \leq 59$ . We see that for any value of the scaled flux  $\gamma$  and the corresponding flux-dependent filling  $N/L = \gamma/2\pi$ , the density oscillations occur at the wavelength corresponding to one particle per oscillation. For example, in the second column we look at  $\gamma = \pi/2$  and the filling  $N/L = 1/4$ , thus implying  $N = 15$  for  $L = 60$ . Here we count 15 full oscillations of the density, each covering four sites. Note that the observed density wave is fundamentally different from a gapped phase with staggered density modulation, which is directly favored by strong nearest-neighbor interactions  $U_2$  and found at half filling [36], since it occurs on longer wave-lengths dictated by the magnetic flux. Nevertheless, a finite value of  $U_2$  enhances the charge gap of the flux-induced density wave. As seen in the plots corresponding to  $\gamma = 2\pi/5$  and  $\gamma = 2\pi/3$ , periodicities of three and five sites are also possible. The

remaining two panels are calculated at  $\gamma = 11\pi/20$  and  $\gamma = 3\pi/4$ . Here, according to the general observed trend one expects an incommensurate filling of, respectively, 16.5 and 22.5 particles per 60 sites. Although the density distributions look less regular in these cases, one still observes the formation of a density wave following the same predictive pattern. The required filling corresponds to the density where the magnetic unit length matches the wavelength of Friedel oscillations [55] in a system of free fermions, to which the simulated system can be mapped for  $t = U_2 = 0$ . Friedel oscillations occur near local defects, such as the boundary of the system, and decay algebraically. It seems that (at finite  $U_2$ ) they are promoted to a long-ranged density wave, when a commensurate magnetic length is introduced with a finite value of  $t$ .

*Summary.*—We described a semi-synthetic zigzag optical lattice built from a one-dimensional spin-dependent optical lattice with transitions between internal atomic states. Each of the lattice’s triangular plaquettes ensnares the same—tunable—magnetic flux that can controllably deform the single-particle band structure from the single-minimum to the double-well configuration. In the proposed setup, the atom-atom interactions are non-local in both dimensions and stabilize density-wave-like phases at flux-dependent filling factors.

We thank Immanuel Bloch, Alessio Celi, Simon Fölling, Sebastian Greschner, Maciej Lewenstein, Michael Lohse, Leonardo Mazza, and Jakub Zakrzewski for helpful discussions. This research was supported by the Lithuanian Research Council (Grant No. MIP-086/2015) and by the German Research Foundation (DFG) via the Research Unit FOR 2414. I. B. S. was partially supported by the ARO’s Atomtronics MURI, by AFOSR’s Quantum Matter MURI, NIST, and the NSF through the PCF at the JQI. C. S. is grateful for support by the Studienstiftung des deutschen Volkes.

---

\* egidijus.anisimovas@ff.vu.lt

† cstraeter@pks.mpg.de

‡ eckardt@pks.mpg.de

§ ian.spielman@nist.gov

¶ gediminas.juzeliunas@tfai.vu.lt

- [1] M. Lewenstein, A. Sanpera, V. Ahufinger, B. Damski, A. Sen (De), and U. Sen, “Ultracold atomic gases in optical lattices: Mimicking condensed matter physics and beyond,” *Adv. Phys.* **56**, 243–379 (2007).
- [2] I. Bloch, J. Dalibard, and W. Zwerger, “Many-body physics with ultracold gases,” *Rev. Mod. Phys.* **80**, 885–964 (2008).
- [3] M. Lewenstein, A. Sanpera, and V. Ahufinger, *Ultracold atoms in optical lattices: Simulating quantum many-body systems* (Oxford University Press, 2012).
- [4] J. Javanainen and J. Ruostekoski, “Optical detection of fractional particle number in an atomic Fermi-Dirac gas,”

*Phys. Rev. Lett.* **91**, 150404 (2003).

- [5] D. Jaksch and P. Zoller, “Creation of effective magnetic fields in optical lattices: the Hofstadter butterfly for cold neutral atoms,” *New J. Phys.* **5**, 56 (2003).
- [6] K. Osterloh, M. Baig, L. Santos, P. Zoller, and M. Lewenstein, “Cold atoms in non-Abelian gauge potentials: From the Hofstadter “moth” to lattice gauge theory,” *Phys. Rev. Lett.* **95**, 010403 (2005).
- [7] J. Dalibard, F. Gerbier, G. Juzeliūnas, and P. Öhberg, “Colloquium: Artificial gauge potentials for neutral atoms,” *Rev. Mod. Phys.* **83**, 1523–1543 (2011).
- [8] N. Goldman, G. Juzeliūnas, P. Öhberg, and I. B. Spielman, “Light-induced gauge fields for ultracold atoms,” *Rep. Prog. Phys.* **77**, 126401 (2014).
- [9] N. Goldman, J. C. Budich, and P. Zoller, “Topological quantum matter with ultracold gases in optical lattices,” *Nat. Phys.* **12**, 639–645 (2016).
- [10] O. Boada, A. Celi, J. I. Latorre, and M. Lewenstein, “Quantum simulation of an extra dimension,” *Phys. Rev. Lett.* **108**, 133001 (2012).
- [11] A. Celi, P. Massignan, J. Ruseckas, N. Goldman, I. B. Spielman, G. Juzeliūnas, and M. Lewenstein, “Synthetic gauge fields in synthetic dimensions,” *Phys. Rev. Lett.* **112**, 043001 (2014).
- [12] H. M. Price, O. Zilberberg, T. Ozawa, I. Carusotto, and N. Goldman, “Four-dimensional quantum Hall effect with ultracold atoms,” *Phys. Rev. Lett.* **115**, 195303 (2015).
- [13] M. Mancini, G. Pagano, G. Cappellini, L. Livi, M. Rider, J. Catani, C. Sias, P. Zoller, M. Inguscio, M. Dalmonte, and L. Fallani, “Observation of chiral edge states with neutral fermions in synthetic Hall ribbons,” *Science* **349**, 1510–1513 (2015).
- [14] B. K. Stuhl, H.-I. Lu, L. M. Ayccock, D. Genkina, and I. B. Spielman, “Visualizing edge states with an atomic Bose gas in the quantum Hall regime,” *Science* **349**, 1514–1518 (2015).
- [15] L. F. Livi, G. Cappellini, M. Diem, L. Franchi, C. Clivati, M. Frittelli, F. Levi, D. Calonico, J. Catani, M. Inguscio, and L. Fallani, “Synthetic dimensions and spin-orbit coupling with an optical clock transition,” (2016), [arXiv:1609.04800 \[cond-mat.quant-gas\]](https://arxiv.org/abs/1609.04800).
- [16] F. A. An, E. J. Meier, and B. Gadway, “Direct observation of chiral currents and magnetic reflection in atomic flux lattices,” (2016), [arXiv:1609.09467 \[cond-mat.quant-gas\]](https://arxiv.org/abs/1609.09467).
- [17] T.-S. Zeng, C. Wang, and H. Zhai, “Charge pumping of interacting fermion atoms in the synthetic dimension,” *Phys. Rev. Lett.* **115**, 095302 (2015).
- [18] S. K. Ghosh, U. K. Yadav, and V. B. Shenoy, “Baryon squishing in synthetic dimensions by effective SU(M) gauge fields,” *Phys. Rev. A* **92**, 051602(R) (2015).
- [19] N. R. Cooper and A. M. Rey, “Adiabatic control of atomic dressed states for transport and sensing,” *Phys. Rev. A* **92**, 021401(R) (2015).
- [20] On a single-particle level, a possibility of creating a non-square semi-synthetic geometry was recently considered by D. Suszalski and J. Zakrzewski, “Different lattice geometries with synthetic dimension,” *Phys. Rev. A* **94**, 033602 (2016). The proposal relies on experimentally more challenging additional diagonal tunnelings between the original sites of a semi-synthetic square lattice.
- [21] D. Greif, G. Jotzu, M. Messer, R. Desbuquois, and

- T. Esslinger, “Formation and dynamics of antiferromagnetic correlations in tunable optical lattices,” *Phys. Rev. Lett.* **115**, 260401 (2015).
- [22] R. G. Hulet, P. M. Duarte, R. A. Hart, and T.-L. Yang, “Antiferromagnetism with ultracold atoms,” (2015), [arXiv:1512.05311 \[cond-mat.quant-gas\]](#).
- [23] M. Boll, T. A. Hilker, G. Salomon, A. Omran, I. Bloch, and C. Gross, “Spin and charge resolved quantum gas microscopy of antiferromagnetic order in Hubbard chains,” (2016), [arXiv:1605.05661 \[cond-mat.quant-gas\]](#).
- [24] L. W. Cheuk, M. A. Nichols, K. R. Lawrence, M. Okan, H. Zhang, E. Khatami, N. Trivedi, T. Paiva, M. Rigol, and M. W. Zwierlein, “Observation of spatial charge and spin correlations in the 2D Fermi-Hubbard model,” (2016), [arXiv:1606.04089 \[cond-mat.quant-gas\]](#).
- [25] T. Lahaye, C. Menotti, L. Santos, M. Lewenstein, and T. Pfau, “The physics of dipolar bosonic quantum gases,” *Rep. Prog. Phys.* **72**, 126401 (2009).
- [26] B. Yan, S. A. Moses, B. Gadway, J. P. Covey, K. R. A. Hazzard, A. Maria Rey, D. S. Jin, and J. Ye, “Observation of dipolar spin-exchange interactions with lattice-confined polar molecules,” *Nature* **501**, 521–525 (2013).
- [27] A. Frisch, M. Mark, K. Aikawa, S. Baier, R. Grimm, A. Petrov, S. Kotochigova, G. Quémener, M. Lepers, O. Dulieu, and F. Ferlaino, “Ultracold dipolar molecules composed of strongly magnetic atoms,” *Phys. Rev. Lett.* **115**, 203201 (2015).
- [28] S. Baier, M. J. Mark, D. Petter, K. Aikawa, L. Chomaz, Z. Cai, M. Baranov, P. Zoller, and F. Ferlaino, “Extended Bose-Hubbard models with ultracold magnetic atoms,” *Science* **352**, 201–205 (2016).
- [29] G. Pupillo, A. Micheli, M. Boninsegni, I. Lesanovsky, and P. Zoller, “Strongly correlated gases of Rydberg-dressed atoms: Quantum and classical dynamics,” *Phys. Rev. Lett.* **104**, 223002 (2010).
- [30] M. Viteau, M. G. Bason, J. Radogostowicz, N. Malossi, D. Ciampini, O. Morsch, and E. Arimondo, “Rydberg excitations in Bose-Einstein condensates in quasi-one-dimensional potentials and optical lattices,” *Phys. Rev. Lett.* **107**, 060402 (2011).
- [31] A. W. Glaetzle, M. Dalmonte, R. Nath, C. Gross, I. Bloch, and P. Zoller, “Designing frustrated quantum magnets with laser-dressed Rydberg atoms,” *Phys. Rev. Lett.* **114**, 173002 (2015).
- [32] H. Labuhn, D. Barredo, S. Ravets, S. de Léséleuc, T. Macrì, T. Lahaye, and A. Browaeys, “Tunable two-dimensional arrays of single Rydberg atoms for realizing quantum Ising models,” *Nature* **534**, 667–670 (2016).
- [33] G. Vidal, “Efficient simulation of one-dimensional quantum many-body systems,” *Phys. Rev. Lett.* **93**, 040502 (2004).
- [34] U. Schollwöck, “The density-matrix renormalization group in the age of matrix product states,” *Ann. Phys.* **326**, 96–192 (2011).
- [35] R. Orús, “A practical introduction to tensor networks: Matrix product states and projected entangled pair states,” *Ann. Phys.* **349**, 117–158 (2014).
- [36] See Supplemental Material for an extended discussion on the construction of the semi-synthetic zigzag lattice, simulations of Bloch oscillations, and the spin polarization induced by strong nearest-neighbor interactions.
- [37] I. H. Deutsch and P. S. Jessen, “Quantum-state control in optical lattices,” *Phys. Rev. A* **57**, 1972–1986 (1998).
- [38] D. McKay and B. DeMarco, “Thermometry with spin-dependent lattices,” *New J. Phys.* **12**, 055013 (2010).
- [39] S. Kolkowitz, S. L. Bromley, T. Bothwell, M. L. Wall, G. E. Marti, A. P. Koller, X. Zhang, A. M. Rey, and J. Ye, “Spin-orbit coupled fermions in an optical lattice clock,” (2016), [arXiv:1608.03854 \[cond-mat.quant-gas\]](#).
- [40] M. L. Wall, A. P. Koller, S. Li, X. Zhang, N. R. Cooper, J. Ye, and A. M. Rey, “Synthetic spin-orbit coupling in an optical lattice clock,” *Phys. Rev. Lett.* **116**, 035301 (2016).
- [41] F. Gerbier and J. Dalibard, “Gauge fields for ultracold atoms in optical superlattices,” *New J. Phys.* **12**, 033007 (2010).
- [42] Y.-J. Lin, K. Jiménez-García, and I. B. Spielman, “Spin-orbit-coupled Bose-Einstein condensates,” *Nature* **471**, 83–86 (2011).
- [43] S. Greschner, L. Santos, and T. Vekua, “Ultracold bosons in zig-zag optical lattices,” *Phys. Rev. A* **87**, 033609 (2013).
- [44] L. Zhou and X. Cui, “Spin-orbit coupled ultracold gases in optical lattices: High-band physics and insufficiency of tight-binding models,” *Phys. Rev. B* **92**, 140502(R) (2015).
- [45] R. Khomeriki and S. Flach, “Landau-Zener Bloch oscillations with perturbed flat bands,” *Phys. Rev. Lett.* **116**, 245301 (2016).
- [46] M. L. Wall and L. D. Carr, “Out-of-equilibrium dynamics with matrix product states,” *New J. Phys.* **14**, 125015 (2012).
- [47] M. Atala, M. Aidelsburger, M. Lohse, J. T. Barreiro, B. Paredes, and I. Bloch, “Observation of chiral currents with ultracold atoms in bosonic ladders,” *Nat. Phys.* **10**, 588–593 (2014).
- [48] In performing calculations we represent the zigzag lattice as a one-dimensional array of sites enumerated consecutively along a zigzag-shaped path.
- [49] M. Piraud, F. Heidrich-Meisner, I. P. McCulloch, S. Greschner, T. Vekua, and U. Schollwöck, “Vortex and Meissner phases of strongly-interacting bosons on a two-leg ladder,” *Phys. Rev. B* **91**, 140406(R) (2015).
- [50] D. Rossini and R. Fazio, “Phase diagram of the extended Bose-Hubbard model,” *New J. Phys.* **14**, 065012 (2012).
- [51] T. Senthil and M. Levin, “Integer quantum Hall effect for bosons,” *Phys. Rev. Lett.* **110**, 046801 (2013).
- [52] S. Furukawa and M. Ueda, “Integer quantum Hall state in two-component Bose gases in a synthetic magnetic field,” *Phys. Rev. Lett.* **111**, 090401 (2013).
- [53] Y.-H. Wu and J. K. Jain, “Quantum Hall effect of two-component bosons at fractional and integral fillings,” *Phys. Rev. B* **87**, 245123 (2013).
- [54] Y.-C. He, S. Bhattacharjee, R. Moessner, and F. Pollmann, “Bosonic integer quantum Hall effect in an interacting lattice model,” *Phys. Rev. Lett.* **115**, 116803 (2015).
- [55] J. Friedel, “Metallic alloys,” *Nuovo Cimento* **7**, 287–311 (1958).

# Semi-synthetic zigzag optical lattice for ultracold bosons

## supplemental material

### A: Tight-binding approximation

In the main text, we consider bosonic atoms with two relevant internal states labeled with the (quasi-)spin index  $s = \pm 1$ . The atoms are confined in one-dimensional periodic trapping potentials, opposite for each internal state,  $V \propto \pm \cos(\kappa x)$ . The two quasi-spin states are coupled by laser-induced transitions characterized by a Rabi frequency  $\Omega$  and a recoil wave vector  $\tilde{\kappa} \mathbf{e}_x$ . Focusing on sufficiently deep lattices, we work within a tight-binding model. We introduce the Wannier functions  $w_j(x)$  localized at the minima  $x_j = aj$  of one-dimensional cosine potential  $V(x) = V_0 \cos(\kappa x)/2$  that oscillates with the periodicity  $a = 2\pi/\kappa$ . The Wannier bases for the two spin states with  $s = \pm 1$  are given by

$$w_{s,j}(x) = w_0(x - sa/4 - ja), \quad (\text{A1})$$

The locations of the opposite spin states differ by  $a/2$ , i. e. by half the lattice constant, and the origin of the  $x$  axis is placed at the midpoint between the neighboring  $s = \pm 1$  sites.

Matrix elements for tunneling along the real dimension have the usual form

$$-t = \int w_{s,j+1}^*(x) \left[ \frac{\hat{p}^2}{2m} - \frac{V_0}{2} \cos(\kappa x) \right] w_{s,j}(x) dx. \quad (\text{A2})$$

With the minus sign absorbed into the definition in Eq. (A2), the quantity  $t$  is real and positive. Matrix elements for tunneling along the two diagonal directions of the semi-synthetic lattice are obtained by overlapping the Wannier functions weighted with the position-dependent laser coupling term:

$$\int w_{1,j}^*(x) \Omega e^{i\tilde{\kappa}x} w_{-1,j}(x) dx = t_D e^{i\tilde{\kappa}aj}, \quad (\text{A3a})$$

and

$$\int w_{1,j+1}^*(x) \Omega e^{i\tilde{\kappa}x} w_{-1,j}(x) dx = t_D e^{i\tilde{\kappa}a(j+1/2)}. \quad (\text{A3b})$$

Here the amplitude  $t_D$  is determined by both the Rabi frequency  $\Omega$  and the overlap integral  $\rho$  between the neighboring Wannier functions for the opposite spin states

$$t_D = \Omega \rho, \quad \rho = \int w_0^*(x - a/4) e^{i\tilde{\kappa}x} w_0(x + a/4) dx. \quad (\text{A4})$$

Within the tight-binding approach, we introduce the Bose operators  $c_{m,j}$  and  $c_{m,j}^\dagger$  to describe the annihilation and creation of atoms on the sites of the semi-synthetic zigzag lattice. By adding appropriate phase factors to these operators  $c_{m,j} \rightarrow c_{m,j} e^{-ijma\tilde{\kappa}/2}$ , one arrives at the tight-binding Hamiltonian with complex-valued tunneling elements along the long direction (real dimension) and real-valued tunneling ( $t_D$ ) along the diagonal semi-synthetic directions:

$$H = t_D \sum_j \left[ c_{1,j}^\dagger c_{-1,j} + c_{1,j-1}^\dagger c_{-1,j} \right] - t \sum_{j,m} c_{m,j+1}^\dagger c_{m,j} e^{-ima\tilde{\kappa}/2} + \text{H.c.} \quad (\text{A5})$$

The semi-synthetic lattice is affected by a non-staggered flux  $\gamma = a\tilde{\kappa}/2 = \pi\tilde{\kappa}/\kappa$  over triangular plaquettes, as illustrated in Fig. 1(a) of the main text.

To take interactions into account, the tight binding Hamiltonian (A5) is complemented with the interaction term

$$H_{\text{int}} = \frac{U_1}{2} \sum_{j,s} n_{s,j}(n_{s,j} - 1) + U_2 \sum_{\langle jj' \rangle} n_{1,j} n_{-1,j'}. \quad (\text{A6})$$

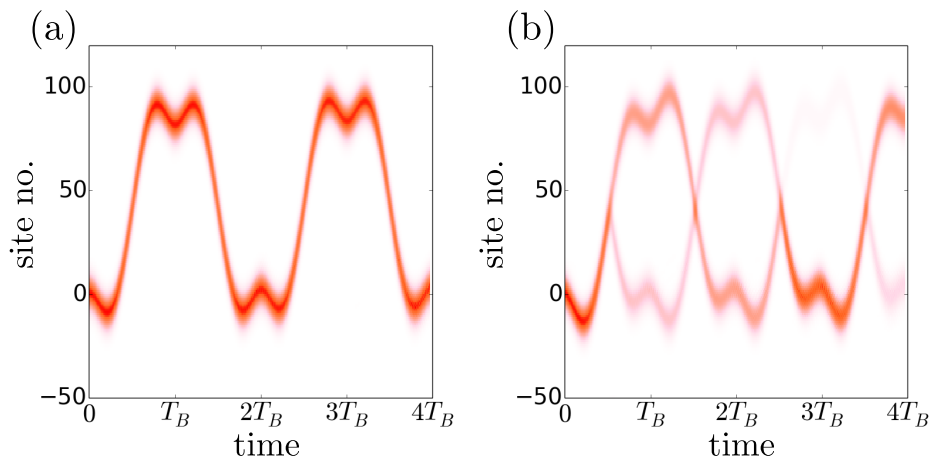


FIG. 4. Bloch oscillations for a Gaussian wave packet in a tilted zigzag lattice. Panel (a) corresponds to the band structure presented in Fig. 2(b) of the main text. In panel (b) the legs of the ladder legs are additionally biased by introducing a spin-dependent onsite energy shift  $\pm 0.3 t\sigma_z$ , and the band gaps opened close to the Brillouin zone boundary lead to the Landau-Zener tunneling between the two bands.

Here

$$U_1 = U_0 \int |w_0(x)|^4 dx \quad (\text{A7})$$

is the onsite interaction energy between atoms with the same spin state. On the other hand,

$$U_2 = U_0 \int |w_0(x + a/4)|^2 |w_0(x - a/4)|^2 dx \quad (\text{A8})$$

represents the density-density interaction between atoms occupying neighboring sites with opposite spin states, i. e., the interactions acting along the diagonal links of the zigzag lattice. The prefactor  $U_0$  is defined by the scattering length (assumed to be state-independent) and the confinement in the perpendicular ( $y$ , and  $z$ ) spatial directions. The specific value of  $U_0$  used in our simulations was obtained for the perpendicular confinement depths of  $30 E_R$ . In Fig. 1(b) of the main text, we plot  $U_1$  and  $U_2$  as a function of the lattice depth showing that  $U_2$  is around five times smaller than  $U_1$  for a typical lattice height  $V_0 = 5 E_R$ . On the other hand, interaction between the atoms at the neighboring sites with the same spin state is much smaller than either  $U_1$  or  $U_2$  and hence is not taken into account.

Coupling to the higher bands becomes relevant for sufficiently strong lasers which couple the states with different band indices and different spins. For instance, for  $V_0 = 5 E_R$  the first and second bands are coupled with a strength  $\Omega \int w_0^*(x - a/4) e^{+i\tilde{k}z} w_0^{(2)}(x + a/4) dx = 0.4935 \Omega$ . Since the gap between the first and the second bands is of the order of  $2E_R$  at  $V_0 = 5E_R$ , the inter-band coupling becomes relevant only for larger  $\Omega$  which is comparable to  $E_R$ , such as for  $\Omega = 0.8E_R$ . This leads to the deviations between the exact and tight binding calculations discussed above. For smaller values of  $\Omega$  one can safely apply the tight-binding model.

## B: Bloch oscillations

To illustrate the observable consequences of symmetry-related doubling of the Brillouin zone, we performed a numerical simulation of a wave packet in the zigzag lattice. We prepared a Gaussian wave packet composed entirely of the states from the lower energy band close to  $k = 0$  and initially situated at a certain position (referred to as site  $j = 0$ ) in the real space. Under the influence of a lattice tilt the wave packet is scanning the single-particle band structure while transferring adiabatically between the two energy bands at the edges of the Brillouin zone. The results of our numerical simulation are shown in Fig. 4(a) for the specific choice  $t_D = t$ , and clearly indicate the doubling of the Bloch period. To clearly illustrate this effect, we contrast these results to those shown in Fig. 4(b). Here, the onsite energies are modified by an additional spin-dependent bias  $0.3 t\sigma_z$  and the single-particle bands acquire small gaps at the Brillouin zone boundaries. As a consequence, the wave packet is split with the atoms being partially transferred into the other band each time the Brillouin zone boundary is reached.

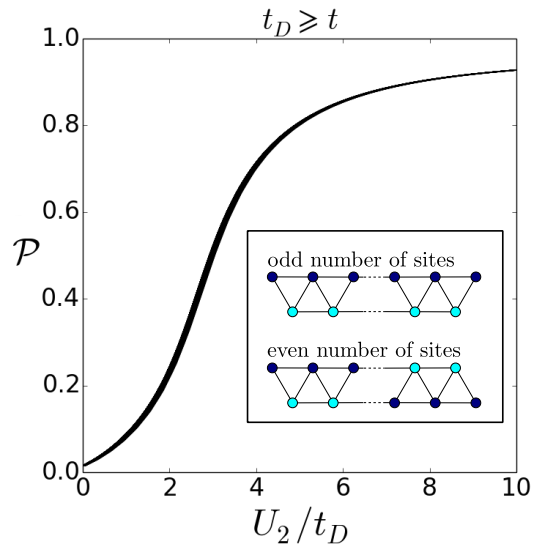


FIG. 5. The spin polarization  $\mathcal{P}$  as a function of the nearest-neighbor repulsion strength calculated for  $N = 30$  particles on a zigzag lattice of  $L = 59$  sites without the artificial flux. When diagonal transitions dominate over the horizontal transitions,  $t_D \geq t$  the shown dependence of the polarization  $\mathcal{P}$  becomes insensitive to the relative magnitude of  $t$ .

### C: Spin polarization

As an example of the many-body physics supported by the zigzag lattice we look at the spin polarization induced by the strong nearest-neighbor interactions. Here, we work at the average filling  $N/L$  close to one half and in the absence of the artificial flux,  $\gamma = 0$ . In the presence of nearest-neighbor interaction — which is a distinguishing feature of the zigzag configuration — the particles are expected to occupy every second site thereby preferentially flocking onto one of the ladder legs and inducing non-zero net spin polarization defined as  $\mathcal{P} = (n_\uparrow - n_\downarrow)/(n_\uparrow + n_\downarrow)$ . A numerical calculation reveals that in this particular case the supported ground state configuration is sensitive to the total number of sites being even or odd. The effect can be explained in a simple way as the tendency of strong interactions to push particles into the sharp corners formed at the ends of the finite lattice. This is illustrated in the inset of Fig. 5 where the dark (light) blue color is used to mark preferentially occupied (depleted) lattice sites. Obviously, if the total number of sites  $L$  is even, the boundary conditions lead to opposite preferred spin polarizations at the two ends of the finite lattice, and the polarization must change sign somewhere in the middle of the lattice. In contrast, when the total number of sites is odd, the boundary conditions facilitate the largely uniform spin polarization of the whole lattice. As a matter of fact, whether or not such a spin-polarized configuration will be formed depends on the competition of the nearest-neighbor repulsion and the delocalizing effect of inter-site hopping. The results of our numerical simulations performed on the system of  $N = 30$  hardcore particles on a lattice of  $L = 59$  sites are presented in Fig. 5. It is striking that as soon as  $t_D \geq t$  the behavior of the spin polarization  $\mathcal{P}$  shows a universal behavior — it depends only on the ratio  $U_2/t_D$  and is virtually independent of the strength of the relatively weaker spin-preserving transitions with the parameter  $t \leq t_D$ . The thick line shown in Fig. 5 is in fact a superposition of many dependencies with the ratio of the hopping parameters  $1 \leq t_D/t \leq 20$ . In the complementary regime  $t \geq t_D$ , spin-preserving hopping transitions start to contribute to the melting of the spin-polarized state. Here, relatively stronger interactions are needed to induce the spin imbalance, and the dependence of the polarization  $\mathcal{P}$  depends on both  $U_2/t$  and  $U_2/t_D$  and thus loses its universal behavior.